

Preliminary evaluation of the correspondence between ion-acoustic signals and luminescence from the absorption of pulsed proton beams in a liquid scintillator

Maria Maxouti*, Peter Hobson**, Oliver Jeremy*, Ben Cox†, Nicholas Dover*, Sonja Gerlach††, Julie Lascaud††, Richard Amos†, Catherine Burne‡, John Civalè**†, Colin Whyte**‡, Jörg Schreiber††, Katia Parodi††, Kenneth Long*, Jeffrey Bamber*†

*Department of Physics, Imperial College London, London, UK. Emails: maria.maxouti@imperial.ac.uk, o.jeremy@imperial.ac.uk, nicholas.dover08@imperial.ac.uk, k.long@imperial.ac.uk

**School of Physical and Chemical Sciences, Queen Mary University of London, London, UK. Email: p.hobson@qmul.ac.uk

†Dept of Med Phys & Biomedical Eng, University College London, London, UK. Emails: b.cox@ucl.ac.uk, r.amos@ucl.ac.uk

††Centre for Advanced Laser Applications (CALA), Faculty of Physics, Ludwig Maximilian Universität, München, Germany. Emails: s.gerlach@physik.uni-muenchen.de, j.lascaud@physik.uni-muenchen.de, joerg.schreiber@lmu.de, katia.parodi@physik.uni-muenchen.de,

‡School of Engineering, University of Birmingham, Edgbaston, UK. Email: CXB1055@student.bham.ac.uk

**†Physics, University of Strathclyde, Glasgow, UK. Email: colin.whyte@strath.ac.uk

*†Division of Radiotherapy and Imaging, Institute of Cancer Research, London, UK. Emails: john.civalè@icr.ac.uk, jeff.bamber@icr.ac.uk

Abstract—For eventual contribution to the subject of radiotherapy with heavy ions, our aim was to advance the field of ionacoustics by establishing the feasibility of using optical images of proton dose deposited in a liquid scintillator as a reference for thermoacoustic measurements in the same liquid. We made the first reported measurements of ultrasound speed and frequency dependent attenuation coefficient of a liquid scintillator, Ultima Gold XR®. We then directed pulsed beams of protons from a laser driven accelerator into a phantom filled with the scintillator while making simultaneous observations of the resulting luminescence and thermoacoustic waves. Preliminary comparisons were obtained between the two, as a function of proton energy and degree of collimation, laying a foundation for future work on 3D ionacoustic dosimetry.

Keywords—Thermoacoustic, laser driven accelerator, liquid scintillator, ultrasound, velocity, attenuation coefficient, radiotherapy, luminescence, dose, measurement and imaging

I. INTRODUCTION

About half of all cancer patients should ideally receive radiotherapy (RT) as part of their treatment [1]. Considerable benefit would therefore result from improved methods to increase the RT dose to cancer cells while sparing healthy tissue. Heavy ions, including protons, have a role in achieving this because (unlike x-rays), they deposit a high dose deep in tissue, at the Bragg peak, controlled by their energy. Interest in generating ion beams for research with flexible choice of ion species, energy, spatial dose pattern and (extremely high) dose rate has led to new accelerators that use pulsed lasers to ionize foil targets [e.g., 2]. The present work is being carried out within a collaboration that aims to develop and exploit such an accelerator [3]. Proton beams from cyclotrons can be electrostatically chopped to deposit their energy in 1-2 μ s, causing the emission thermoacoustic waves [4]. However, laser-driven accelerators can deposit their dose per pulse within tens of nanoseconds, which facilitates efficient coupling to thermoacoustic waves [5]. With further development, ionacoustic imaging offers potential for real-time localisation

of the Bragg peak during treatment and 3D dose maps overlaid on images of the body. The present work aims to advance the field of acoustic mapping of ion dose distributions by establishing the feasibility of employing optical images of the dose deposited in a liquid scintillator as a pulse-by-pulse calibration reference for acoustic observations in the same liquid.

II. METHODS

A. Phantom

A phantom was developed to be filled with a liquid scintillator (Ultima Gold XR™, Scientific Laboratory Supplies Ltd., Nottingham, UK), with an air-filled proton beam entry port and five observation ports, three acoustic and two optical (Figs. 1 and 2). The entry port and two of the acoustic ports were sealed by 50- μ m black Kapton® (polyimide) foils (Goodfellow, Cambridge, UK). The remaining acoustic port was for an immersion transducer. Both optical ports allowed direct observation of scintillation light via digital cameras and a bespoke lens system.

B. Acoustic characterisation of Kapton foil and scintillator

Prior to phantom construction, measurements were made of ultrasound transmission through the Kapton foil and the liquid scintillator, to provide confidence that neither would substantially impede or disturb acoustic transmission.

The phantom design relied upon acoustic coupling from the liquid scintillator to the ultrasound transducers at Kapton-foil ports with the aid of ultrasound coupling gel. The combination of Kapton and ultrasound coupling gel applied as it would be during the proton-beam experiment was therefore characterised, in terms of both transmission loss and potential for wavefront distortion. A 32x32-element, 3.5-MHz matrix array transducer (Verasonics Inc., Kirkland, USA) was pressed against a blob of coupling gel in the centre of a replica Kapton window. Using plane transmitted ultrasound waves, echoes from a 2.5-cm diameter bronze sphere were detected on all 1024 elements of the array. A large sphere was used because it acts as specular reflector,

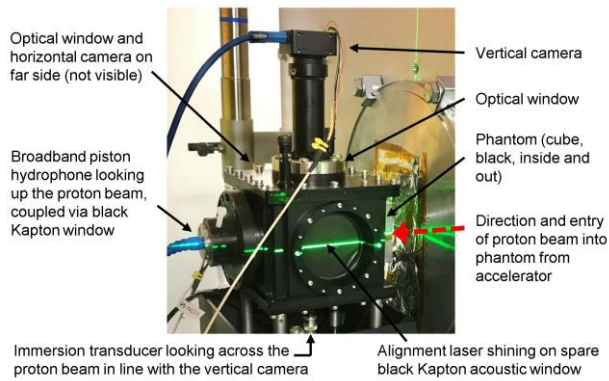


Fig. 1. Liquid scintillator-filled phantom in position ready for the proton beam to enter via the air-filled entry port show in Fig. 2.

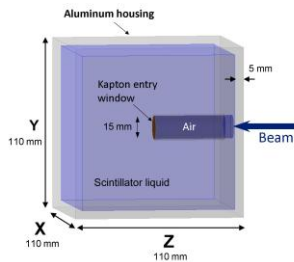


Fig. 2. Outline of the phantom showing the proton beam entry port.

does not require alignment to the wavefronts, and the echo analysis would be tolerant to some lateral mispositioning. Fig. 3 shows the arrangement, without and with the Kapton window in place. Fig. 4 shows example radiofrequency echo acquisitions on the central row of 32 elements, before and after time-alignment using the interpolated peak of the normalised cross-correlation function calculated between the signal on each element and the element with earliest time of arrival. The time-aligned echoes from all 1024 elements were used to estimate the wave amplitude spatially averaged over an area of the Kapton foil similar to that covered by either of the transducers used in the experiment with pulsed beams of protons. Wavefront distortion over this area was characterized by comparing spatial coherence functions [6], calculated as the normalised cross-correlation coefficient after time-alignment between the voltage-time waveform on each element and that on the element with the earliest arrival, with and without the Kapton-gel window.

The speed and attenuation coefficient of ultrasound in Ultima Gold XR was measured using the insertion method [7] (Fig. 5). The liquid scintillator was contained within a Perspex® cylinder (56 mm internal diameter) having Mylar®

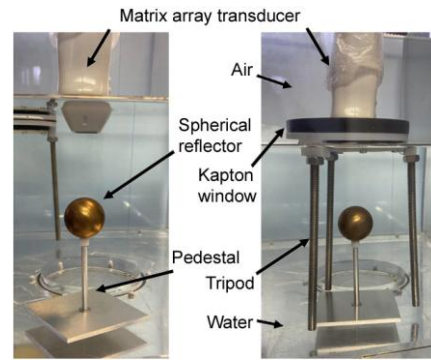


Fig. 3. Experiment to compare ultrasound transmission through water (left) with that through a Kapton-gel window (right).

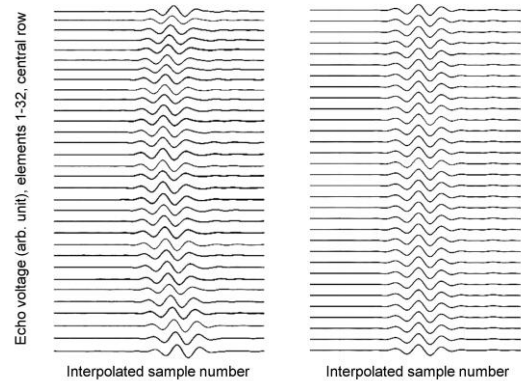


Fig. 4. Examples of echo signals from the sphere on the centre-row elements of the array, before (left) and after (right) time alignment.

acoustic windows and placed centrally between two weakly-focused confocal disc transducers (each radius 1 cm, beam width ~ 5 mm), one transmitting and the other receiving. The transmitting transducer was excited by a short high-voltage impulse, producing a ~ 2.5 -cycle acoustic pulse of centre frequency ~ 2.5 MHz. Voltage signals from the receiving transducer, digitised by a PicoScope 5000®, were analysed by fast Fourier transform in Matlab, and peak pulse arrival-time detection. Frequency dependent signal amplitude and pulse arrival time were measured for water as a reference and with the sample (59-mm pathlength) inserted as shown in Fig. 5. The attenuation coefficient over the frequency range 1.5 – 3.5 MHz and speed of sound were calculated as described in [6], disregarding losses due to the Mylar and the water-Ultima Gold XR interface (estimated as negligible given Ultima Gold XR's density of 1.005 g/cm^3 [8] and sound speed reported below). The measurements were made with the liquids at room temperature (21.8°C).

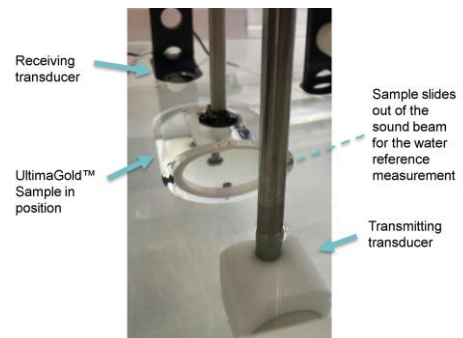
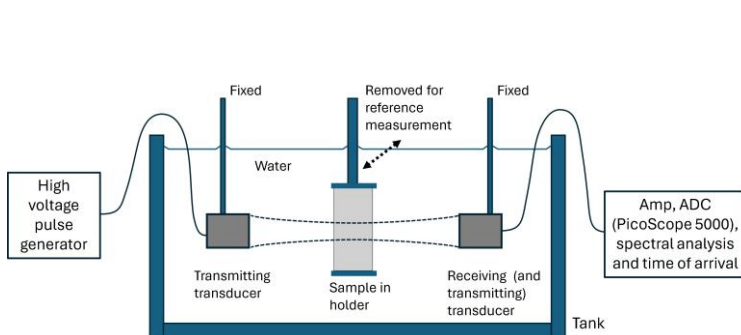


Fig. 5. Diagram (left) and photograph (right) of the apparatus used to measure ultrasound speed and attenuation coefficient of Ultima Gold XR.

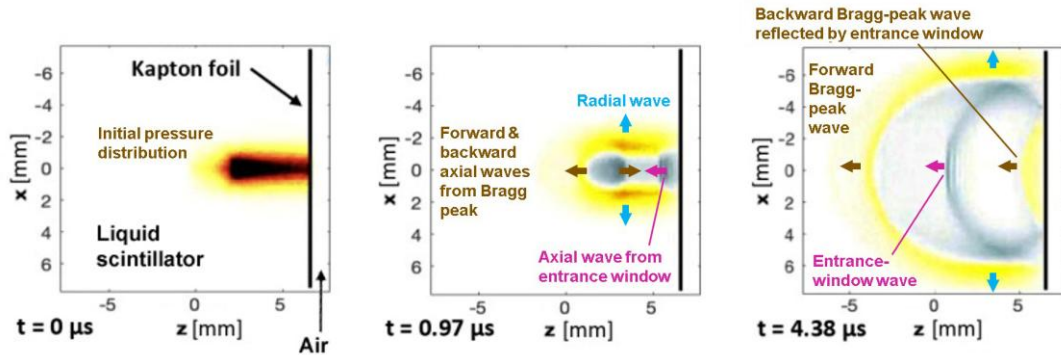


Fig. 6. Frames from a k-Wave simulation movie: the initial acoustic pressure from the energy deposited by a proton beam entering the liquid scintillator via the air-Kapton window (left), key thermoacoustic wave components soon after emission (middle), the axial and radial waves that eventually arrive at the piston hydrophone and immersion ransducer respectively(right). Colours: positive pressure in yellow-red, negative in grey.

C. Experiment with pulsed beams of protons

Protons produced by a pulsed laser focused onto a water leaf, in the laser-driven ion (LION) accelerator at CALA, Munich, were directed into the phantom via its entrance port. Although the laser can generate 2.5 PW, for this experiment powers of about 0.3 PW were used. The two cameras were positioned perpendicular to each other and to the proton beam axis (Fig. 1). A broadband plane piston 25-mm diameter hydrophone (ML4X50, Precision Acoustics, Dorchester, UK), coupled via a Kapton-gel window, was located on the proton beam axis pointing towards the source. The hydrophone has a flat response ± 1.5 dB calibrated from 100 kHz to 1 MHz, with good sensitivity to many MHz. An Olympus 1-MHz 13-mm diameter plane disc immersion transducer (V303, Evident Scientific, Stansted, UK) was positioned close to the entry window, receiving perpendicular to the beam axis. Its nominal 6-dB bandwidth was 0.5 – 1.5 MHz. For successive proton beam pulses, simultaneous observations were made of luminescence and acoustic waves detected as function of incident nominal proton energy (10 – 20 MeV) and beam width (generated by collimator diameters 2 and 4 mm, and uncollimated).

D. Simulations to assist design and interpretation of results

A simulation pipeline was established consisting of a BDSIM [9] model of the LION beamline. Particle transport through the entrance port and in the liquid scintillator was modelled using Monte Carlo methods in Geant4 [10], producing 3D deposited-energy distributions for protons, secondary particles and electrons. The contribution from protons was about $\times 10^4$ that of the other particles. The total deposited energy was converted to a 3D acoustic pressure impulse and the resulting acoustic waves propagated and visualised in k-Wave [11]. Fig. 6 shows three frames from a

k-Wave movie, labelled with the main wave components that arrive at the piston hydrophone (imagined left of each diagram, on the beam axis “looking” towards the source) and the immersion transducer (imagined bottom of each diagram, “looking” across the beam radius). The simulations were used to assist interpretation of the experimentally recorded waveforms.

Ray-tracing simulations with Ansys Zemax OpticStudio (Cambridge, UK) helped design the optics for scintillation imaging and assist interpretation of the images [12].

III. RESULTS

A. Kapton membrane

Fig. 7 shows three repeats, with and without a Kapton-gel window, of the mean and standard deviation after time-alignment of all 1024 matrix-array echo signals from the reflecting sphere. Accounting for both transmit and receive acoustic paths, the window was found to attenuate the 3.5-MHz pulse by 1.4 ± 0.23 dB. No significant loss of spatial coherence was observed (data not shown).

B. Liquid scintillator

The acoustic attenuation coefficient of Ultima Gold XR at 21.8°C was found to vary as $0.19 \pm 0.002 f^{1.75 \pm 0.01}$ dB/cm, where f is frequency in range 1.5 – 3.5 MHz and the errors represent \pm one standard deviation. The speed of sound was found to be 1479.1 ± 1.1 m/s, where the error was approximated from half the range of observed values.

C. Acoustic and scintillation emissions

Example scintillation images and acoustic waveforms are provided in Fig. 8, for selected proton energies and collimation conditions. The figure is labelled to show various wave components that were illustrated in Fig. 6. Knowing the speed of sound in Ultima Gold XR, the Bragg peak range was measured from the time separation of wave components arriving at the piston hydrophone from the Bragg peak, the entrance window and the Bragg-peak after reflection by the entrance window [5]. The proton beam width was estimated from the wave components arriving at the immersion transducer from the near edge and the far edge of the beam.

The analysis to compare the acoustic data with data from the luminescence images is ongoing due to a discovery that a flange on the phantom’s entrance window seal had prevented some scintillation light reaching the cameras. A preliminary

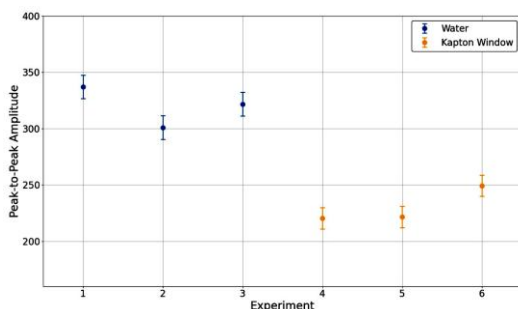


Fig. 7. Means and standard deviations of echoes from the spherical reflector with and without the Kapton window interposed.

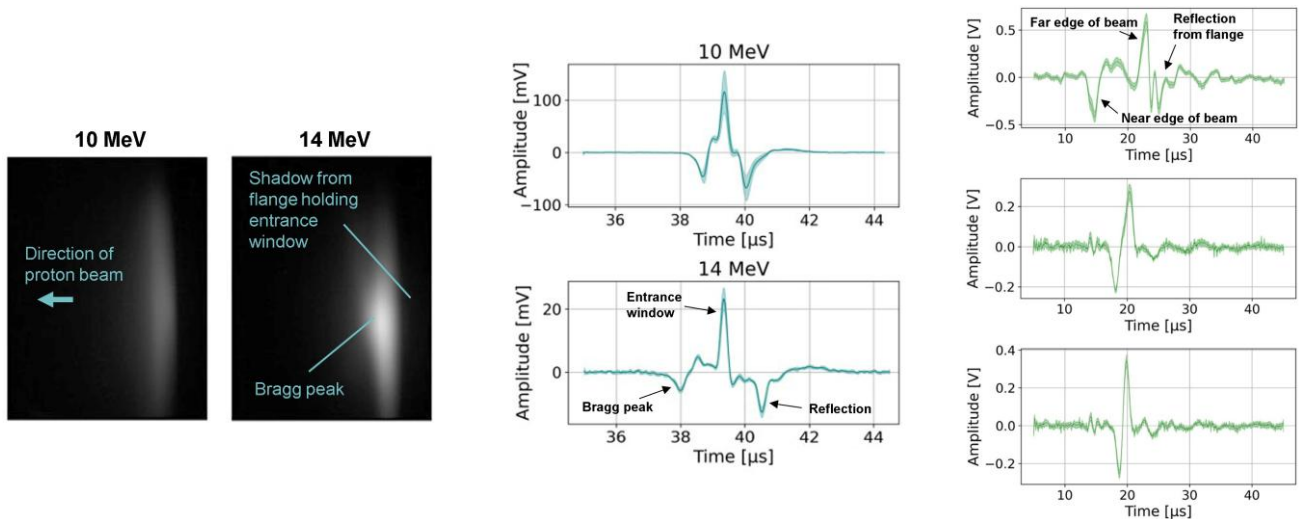


Fig. 8. Example scintillation images with no collimator (left), and acoustic waveforms (middle and right) averaged with error bounds for 2-5 pulses. The time separation between the labelled waveform components received by the piston hydrophone for 14 MeV (bottom-middle) is greater than that for 10 MeV (top-middle) because the Bragg-peak range increases with energy (beams uncollimated). The waveform components for the immersion transducer become progressively closer, moving from an uncollimated beam (top-right), to 4-mm (middle-right) and 2-mm collimation (bottom-right).

subjective interpretation of the scintillation images appeared to show that the optically detected Bragg-peak range followed a similar trend with proton design energy to that detected acoustically. Similar trends were also seen between optical and acoustic estimates of proton beam width under varying collimation. To enable a quantitative approach that will be free of potential for observer bias, optical ray-tracing simulations and calibrations of camera response are currently being conducted with the aims, if possible, of (a) deriving factors that will correct for the shadowing, (b) provide quantitative measurements of Bragg-peak range and beam width, and (c) enable pulse-by-pulse comparison of luminescence intensity with acoustic wave amplitude.

IV. DISCUSSION

The first reported measurements of the acoustic characteristics of Ultima Gold XR were made, providing confidence that ionoacoustic waves would be measurable through the scintillator. This was confirmed by the first simultaneous optical and acoustic measurements of pulsed proton beam dose patterns in a liquid scintillator. Further acoustic measurements to assist such work should include studying the attenuation coefficient of the scintillator over a wider frequency range and measuring its acoustic nonlinearity parameter.

A more detailed ray-tracing simulation is underway with the aim of correcting for the effect of the flange shadow, to enable objective optical measurements of Bragg-peak range and beam width. Meanwhile the results presented here provide preliminary evidence that, with an improved phantom design, the generation of ionoacoustic waves within a liquid scintillator should allow optical validation and calibration of ionoacoustic proton beam dosimetry on a pulse-by-pulse basis. As such, this study lays a foundation for future work using wideband arrays for full 3D ionoacoustic reconstruction of dose distributions.

REFERENCES

- [1] Wakeham K, Cooper T, Quinlan S. World-class radiotherapy in the UK. All Party Parliamentary Group for Radiotherapy, Radiotherapy UK. <https://radiotherapy.org.uk/wp-content/uploads/2024/02/Radiotherapy-WorldClass-WEB.pdf> [Accessed 22nd August 2025]
- [2] Kroll, F, Brack FE, Bernert C, Boch S, Bodenstern, E, Brüchner K et al. Tumour irradiation in mice with a laser-accelerated proton beam. *Nat. Phys.* 18, 316–322, 2022.
- [3] Aymar G, Becker T, Boogert S, Borhgesi M, Bingham R, Brenner C, et al. LhARA: The Laser-hybrid Accelerator for Radiobiological Applications. *Front Phys.* 8:567738, 2020.
- [4] Mast TD, Johnstone DA, Dumoulin CL, Lamba MA, Patch SK. Reconstruction of thermoacoustic emission sources induced by proton irradiation using numerical time reversal. *Phys. Med. Biol.* 68, 025003, 2023.
- [5] Schauer J, Wieser H-P, Huang Y, Ruser H, Lascaud J, Würfl M, et al. Proton beam range verification by means of ionoacoustic measurements at clinically relevant doses using a correlation-based evaluation. *Front. Oncol.* 12:925542, 2022.
- [6] Bamber JC, Mucci RA, Orofino DP. Spatial coherence and beamformer gain. pp. 43-48 in: Lee H. (ed.) *Acoustical Imaging*, Vol. 24, Kluwer Academic / Plenum Press, New York, 2000.
- [7] Bamber JC. Attenuation and absorption Ch.4 pp.93-166 in: Hill CR, Bamber JC, ter Haar GR (eds.) *Physical Principles of Medical Ultrasonics*, ISBN 978-047197002-6, John Wiley, Chichester, 2004.
- [8] Ultima Gold XR Safety Data Sheet, Revvity. [https://resources.revvity.com/pdfs/MSDS_6013119_Ultima_Gold_XR_\(AU\).pdf](https://resources.revvity.com/pdfs/MSDS_6013119_Ultima_Gold_XR_(AU).pdf). [Accessed 28th August 2025].
- [9] Nevay LV, Boogert ST, Snuverink J, Abramov A, Deacon LC, Garcia-Moralis H, et al. BDSIM: An accelerator tracking code with particle-matter interactions. *Computer Physics Communications*, 252, 107200, 2020.
- [10] Agostinelli S, Allison J, Amako K, Apostolakis J, Araujo H, Arce P, et al. Geant4 - A Simulation Toolkit. *Nucl Instrum Meth A*, 506:250-303, 2003.
- [11] Treeby BE, Cox BT. k-Wave: MATLAB toolbox for the simulation and reconstruction of photoacoustic wave fields. *Journal of Biomedical Optics*, 15:021314, 2010.
- [12] Hobson P, Maxouti M, Bamber J, Long K. Imaging the energy deposited by a 20 MeV proton beam using a commercial liquid scintillator, in: *Optica Imaging Congress 2024 (3D, AOMS, COSI, ISA, pcAOP)*, Technical Digest Series (Optica Publishing Group, 2024), paper IW1D.4. <https://opg.optica.org/viewmedia.cfm?uri=ISA-2024-IW1D.4&seq=0>.